



Effective magnetic fields induced by chiral phononsGuohuan Xiong ^{1,2,3} Hao Chen,^{1,4} Dengke Ma ^{1,*} and Lifa Zhang^{1,†}¹*Phonon Engineering Research Center of Jiangsu Province, Center for Quantum Transport and Thermal Energy Science, Institute of Physics Frontiers and Interdisciplinary Sciences, School of Physics and Technology, Nanjing Normal University, Nanjing 210023, China*²*School of Physical Science and Technology, Yangzhou University, Yangzhou 225002, China*³*Department of Physics, National University of Singapore, Singapore 117551, Singapore*⁴*Department of Physics, University of Science and Technology of China, Hefei 230026, China*

(Received 30 September 2021; revised 2 August 2022; accepted 21 September 2022; published 4 October 2022)

In a semiclassical model, magnetic fields can originate from the orbital magnetic moments of electrons. Here, using the Biot-Savart law, we theoretically predict the effective magnetic fields induced by chiral phonons in the point-charge model. Taking tellurium as an example, it is found that by applying a temperature gradient, the average effective magnetic field per mode for a specific location within a unit cell can reach the order of 0.01 T at room temperature. We prove that the effective magnetic field induced by chiral phonons has the ability to manipulate the Curie temperature and spontaneous magnetization in a ferromagnetic material or even in a general material.

DOI: [10.1103/PhysRevB.106.144302](https://doi.org/10.1103/PhysRevB.106.144302)**I. INTRODUCTION**

A magnetic field, a vector field in which magnetic forces are observable, can interact with moving electric charges, current, and magnetic materials [1,2]. Nowadays, technologies utilizing magnetic field, such as electric generators [3], power transformers [4], magnetic recordings [5], and magnetic confinement fusion [6], have become essential for electrical, information, and energy industries. In a semiclassical model, the magnetic field can be generated by the electron orbiting around a nucleus, which originates from the orbital magnetic moment of the electron [1]. This point has been thoroughly discussed during the past century [7]. As another energy carrier, can it be used to generate magnetic fields?

Phonons, quanta of lattice vibrations, have been proved to possess various properties similar to electrons [8–11]. At present, it has been confirmed that phonons are able to do circular or elliptical rotation, which is known as chirality [12,13]. Chiral phonons widely exist in systems with threefold rotational symmetry and spatial inversion symmetry breaking [10,14–18]. Similar to the chirality of electrons, the chiral phonons can be endowed with pseudoangular momentum due to the threefold rotational symmetry at the high-symmetry points [13,19,20]. Thus, phonons have the ability to switch the electronic valley and can be involved in optical processes [15,21–30].

Although phonons are neutral particles, they can be indirectly connected with magnetic phenomena, such as phonon Hall effect [31–33]. By applying a temperature gradient to deviate the distribution function of phonons from equilibrium, a net phonon angular momentum can be generated [34], and

even the phonon angular momentum Hall effect [35] can appear. Linked to the phonon angular momentum, for a sublattice with nonzero Born effective charge tensor, the circular motion of each site can induce magnetic moment [36]. Thus, in one unit cell, the magnetic moment is given by the sum of the moments caused by each site. At present, phonon magnetic moment has also been reported to be obtained by laser excitations [37–42], external magnetic fields [43,44], electric fields [45], circular fluctuation of ferroelectric phonons at a quantum critical point [46], and topological magnetization [47]. In this scenario, magnetic fields are expected to be generated by phonon chiralities in many ways.

However, recent experiments [39,43] reported that the phonon magnetic moment is 3 to 4 orders of magnitude smaller than previous theoretical calculation [36]. This may be because the g factor used in previous calculation needs to be corrected [43,47,48]. Therefore, more theoretical research on this physical phenomenon is still needed. For example, how much role can the circular current caused by the phonon chiral motion play in the effective magnetic moment? Does the interaction between the chiral phonons magnetic moments affect the measurement? In other words, what order of magnitude can the effective magnetic field induced by the phonon chiral motion reach? What is the spatial distribution of the effective magnetic field? What is the strength of the superposition effect of the effective magnetic field? All these are worthy of further study.

In this paper, under the Born-Oppenheimer approximation, we theoretically predict the effective magnetic fields induced by chiral phonons using the Biot-Savart law. We adopt Te (tellurium) as an example. A temperature gradient is applied to generate an effective magnetic field. The effective phonon magnetic field in a ferromagnetic material and a general material may have the potential to manipulate spontaneous magnetization.

*dkma@njnu.edu.cn

†phyzlf@njnu.edu.cn

II. METHOD

Assuming an elliptical vibration induced by sublattice j , the chiral phonon can be characterized by circular polarization along α direction as [13]

$$s_j^\alpha = \epsilon^\dagger \hat{S}_j^\alpha \epsilon \hbar. \quad (1)$$

Here, ϵ is the phonon eigenvector. \hat{S}_j^α is the operator of phonon circular polarization along α direction for sublattice j , and it has elements of $(\hat{S}_j^\alpha)_{\alpha_1\alpha_2} = (-i)\epsilon_{\alpha\alpha_1\alpha_2} \otimes (A_j)_{N \times N}$ ($\alpha, \alpha_1, \alpha_2 = x, y, z$) for a unit cell with N atoms. ϵ is the Levi-Civita symbol. $(A_j)_{N \times N}$ is a diagonal matrix with elements $(A_j)_{jj'} = \delta_{j,j'}$ for the j th atom. For a positive circular polarization, the phonon mode is right-handed circularly or elliptically polarized; for a negative circular polarization, the phonon mode is left-handed circularly or elliptically polarized; otherwise, it is static or linearly polarized. For simplicity, the plane perpendicular to α direction is set as α^\perp plane.

Phonon polarization s_j^α has the same form as the corresponding phonon angular momentum l_j^α . In equilibrium, the average phonon angular momentum per mode can be represented as [44]

$$L_{eq}^\alpha = \frac{1}{N_{\text{mode}}} \sum_k \sum_j l_j^\alpha(k) \left[f_0(\omega_k) + \frac{1}{2} \right], \quad l_j^\alpha = s_j^\alpha \quad (2)$$

where N_{mode} is the total phonon mode number in the first Brillouin zone, $f_0(\omega_k) = 1/(e^{\frac{\hbar\omega}{k_B T}} - 1)$ is the Bose-Einstein distribution, and $k = (\mathbf{k}, \sigma)$ specifies a wave vector \mathbf{k} and a band σ . The summation here only covers all the positive phonon branches.

In the case of the point-charge model, similar to the electronic circular current, for the sublattice with nonzero effective charge,

$$Z_{j,\alpha^\perp}^*(\sigma) = \frac{\sum_{\alpha' \neq \alpha} Z_{j,\alpha\alpha'}^* \epsilon_{j,\alpha'}(\mathbf{k} = 0, \sigma)}{\left\{ \sum_{j,\alpha'} [\epsilon_{j,\alpha'}(\mathbf{k} = 0, \sigma)]^* \epsilon_{j,\alpha'}(\mathbf{k} = 0, \sigma) \right\}^{1/2}}, \quad (3)$$

where $Z_{j,\alpha\alpha'}^*$ is the Born effective charge [49] in direction α caused by an atomic displacement in direction α' . A steady current $I_j^{\alpha^\perp}(k)$ in α^\perp plane induced by the rotation of phonon can be described as

$$I_j^{\alpha^\perp}(k) = Z_{j,\alpha^\perp}^*(\sigma) \omega_k \frac{l_j^\alpha(k)}{|l_j^\alpha(k)|}. \quad (4)$$

The group velocity of phonon is much smaller than that of photon. For a phonon mode with a wave vector \mathbf{k} and the σ th band, assuming an elliptical trajectory with a major semiaxis $r_{ma,j}^{\alpha^\perp}(k)$ and a minor semiaxis $r_{mi,j}^{\alpha^\perp}(k)$, we can mathematically treat it as a circle with an effective radius $\tilde{r}_j^{\alpha^\perp}(\mathbf{k}, \sigma) = \sqrt{r_{ma,j}^{\alpha^\perp}(\mathbf{k}, \sigma) r_{mi,j}^{\alpha^\perp}(\mathbf{k}, \sigma)}$, which is independent of the system temperature T but only depends on $\epsilon_{k,\sigma} \sqrt{\hbar/\omega_{k,\sigma}}$ [50]. As shown in Fig. 1, a place i is a distance $d_{ij}^{\alpha^\perp}$ above α^\perp plane and a distance d_{ij}^{α} away from the center axis of the elliptical loop produced by atom j . Adopting the Biot-Savart law [1], the magnetic field along α direction at a place i , can be

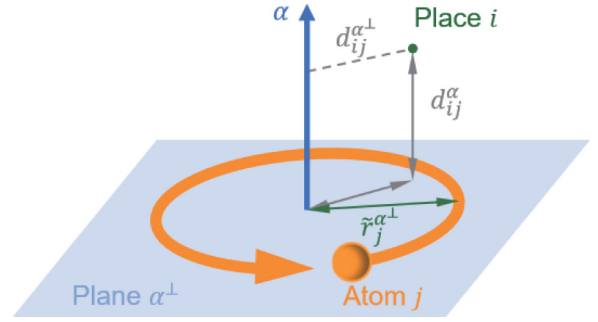


FIG. 1. Schematic of chiral phonon effective magnetic field β_{ij}^α . If $r_{ma,j}^{\alpha^\perp}(k)$ and $r_{mi,j}^{\alpha^\perp}(k)$ are the major and minor semiaxes of an elliptical trajectory, respectively, we can mathematically treat the elliptical trajectory as a circle with an effective radius $\tilde{r}_j^{\alpha^\perp}(\mathbf{k}, \sigma) = \sqrt{r_{ma,j}^{\alpha^\perp}(\mathbf{k}, \sigma) r_{mi,j}^{\alpha^\perp}(\mathbf{k}, \sigma)}$ to calculate a magnetic field along α direction at a place i , i.e., β_{ij}^α . The place i is a distance $d_{ij}^{\alpha^\perp}$ above α^\perp plane and a distance d_{ij}^{α} away from the center axis of the elliptical loop produced by atom j .

obtained as

$$\beta_{ij}^\alpha(k) = \frac{\mu_0}{2\pi} I_j^{\alpha^\perp}(k) \tilde{r}_j^{\alpha^\perp}(k) \Theta_{ij}^{\alpha^\perp}, \quad (5)$$

where μ_0 is the vacuum permeability:

$$\Theta_{ij}^{\alpha^\perp}(k) = \int_0^\pi [\tilde{r}_j^{\alpha^\perp}(k) + d_{ij}^{\alpha^\perp} \cos \theta] d\theta / \left\{ [\tilde{r}_j^{\alpha^\perp}(k)]^2 + (d_{ij}^{\alpha^\perp})^2 + (d_{ij}^{\alpha})^2 + 2\tilde{r}_j^{\alpha^\perp}(k) d_{ij}^{\alpha^\perp} \cos \theta \right\}^{\frac{3}{2}}. \quad (6)$$

Then, the phonon magnetic field along the α direction at place i , induced by a phonon mode with a wave vector \mathbf{k} and the σ th band, can be given by summing the phonon magnetic fields generated by all sublattices around the place i . That is,

$$\beta_i^\alpha = \sum_j \beta_{ij}^\alpha. \quad (7)$$

Since the distribution of $l_j^\alpha(k)$ equals to $[f_0(k) + \frac{1}{2}]$, in equilibrium, the average effective phonon magnetic field per mode at place i is equal to

$$B_{i,eq}^\alpha = \frac{1}{N_{\text{mode}}} \sum_k \beta_i^\alpha(k) \left[f_0(\omega_k) + \frac{1}{2} \right]. \quad (8)$$

With time-reversal symmetry, one can obtain [44] $\omega_{-\mathbf{k},\sigma} = \omega_{\mathbf{k},\sigma}$ and $\epsilon_{-\mathbf{k},\sigma} = \epsilon_{\mathbf{k},\sigma}^*$. Then, we have $l_j^\alpha(-\mathbf{k}, \sigma) = -l_j^\alpha(\mathbf{k}, \sigma)$ and $\tilde{r}_j^{\alpha^\perp}(-\mathbf{k}, \sigma) = \tilde{r}_j^{\alpha^\perp}(\mathbf{k}, \sigma)$. Thus, for a system with time-reversal symmetry, the average effective magnetic field induced by chiral phonons is zero.

In nonequilibrium, we focus on a linear response regime with infinitely small heat current, and assume a constant relaxation time τ . On the base of Boltzmann transport theory, the distribution function deviating from Bose-Einstein distribution is given as [34,51]

$$f(\omega_k) = f_0(\omega_k) - \tau v_k^\alpha \frac{\partial f_0}{\partial T} \frac{\partial T}{\partial \mathcal{L}_\alpha}, \quad (9)$$

where v_k^α is the group velocity of each phonon mode and equals to $\partial\omega_k/\partial k_\alpha$. $\frac{\partial T}{\partial \mathcal{L}_\alpha}$ is the temperature gradient along the

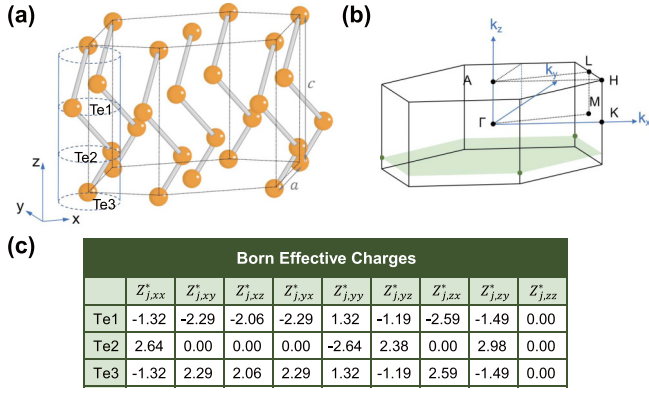


FIG. 2. (a) Crystal structure, (b) the first Brillouin zone, and (c) Born effective charges of Te. The green plane and dots indicate $k_z a/2\pi = -\frac{1}{5}$ and $(ka/2\pi) = [\frac{1}{3}, \frac{1}{3}, -\frac{1}{5}]$, respectively. The unit of $Z_{j,\alpha\alpha'}^*$ is e .

α direction. Finally, the average magnetic field per mode at place i induced by temperature gradient is

$$B_{i,neq}^{\alpha\alpha'} = -\frac{\tau}{N_{\text{mode}}} \sum_{\sigma>0,k} \beta_i^\alpha(\mathbf{k}, \sigma) v_k^{\alpha'} \frac{\partial f_0(\omega_{k,\sigma})}{\partial T} \frac{\partial T}{\partial \mathcal{L}_{\alpha'}} \equiv \gamma_i^{\alpha\alpha'} \frac{\partial T}{\partial \mathcal{L}_{\alpha'}}, \quad (10)$$

where $\gamma_i^{\alpha\alpha'}$ is a linear response coefficient. Therefore, the generated phonon magnetic field is proportional to the temperature gradient.

III. STRUCTURE

As an example, we consider Te (tellurium), a chiral semiconductor at ambient pressure with a helical crystal structure. As depicted in Fig. 2, a trigonal crystal structure is formed by the helical chains, which have three atoms per unit cell. The screw symmetry considered in this paper is right handed, corresponding to the space group of $P3_121$ (D_3^4). The phonon frequencies and eigenvectors are calculated by the density functional perturbation theory using the Vienna *ab initio* simulation package (VASP) [52] with projector augmented-wave (PAW) pseudopotential [53]. The generalized gradient approximation [54] is used for the exchange-correlation function and a plane-wave energy cutoff of 60 Ry is employed. The optimized unit-cell parameters are $a = 4.51$ Å and $c = 5.96$ Å. The internal atomic position parameter is $u = 0.268$ Å. A $9 \times 9 \times 16$ \mathbf{k} -point mesh is applied. The Born effective charge tensor of each atom is shown in Fig. 2(c), which obeys the acoustic sum rule [55].

IV. RESULTS

A. Chiral phonon effective magnetic field

Figure 3 presents the trajectories of three atoms in one unit cell for the highest band at $(ka/2\pi) = [\frac{1}{3}, \frac{1}{3}, -\frac{1}{5}]$, which is the point shown in Fig. 2(b). The chiral phonons in Te usually do elliptical rotation. The plane $k_z a/2\pi = -\frac{1}{5}$ and the point $(ka/2\pi) = [\frac{1}{3}, \frac{1}{3}, -\frac{1}{5}]$ marked in Fig. 2(b) are chosen because

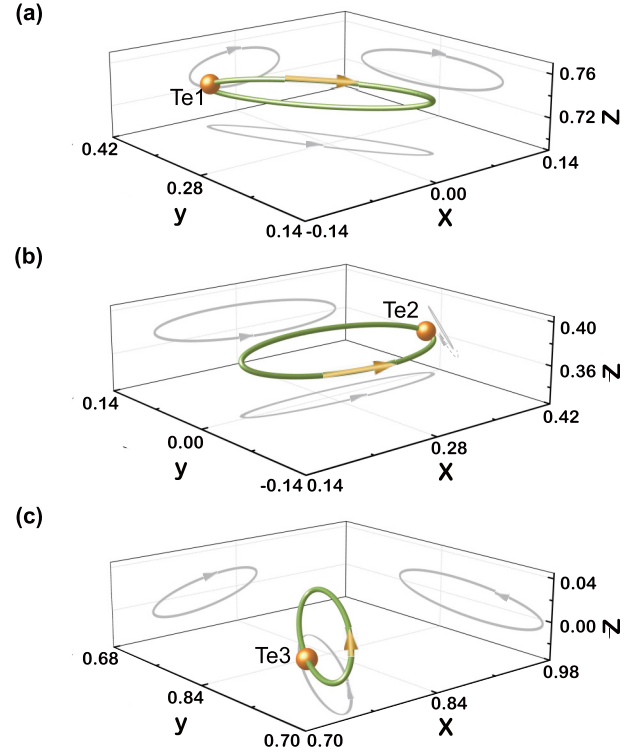


FIG. 3. Trajectories of the three atoms in the unit cell of Te for the phonon of the highest band at $(ka/2\pi) = [\frac{1}{3}, \frac{1}{3}, -\frac{1}{5}]$. The units of the axes are Å.

the normalized trajectory at $(ka/2\pi) = [\frac{1}{3}, \frac{1}{3}, -\frac{1}{5}]$ point has a triple rotational symmetry along the z direction. Here, as shown in Fig. 4, the phonon circular polarization is an odd function in \mathbf{k} space. Figure 4(a) shows that owing to the three-fold screw symmetry of space, one can get Fig. 4(a) or 4(c) by rotating Fig. 4(b) counterclockwise or clockwise along the z axis. The phonon circular polarizations for the three atoms per

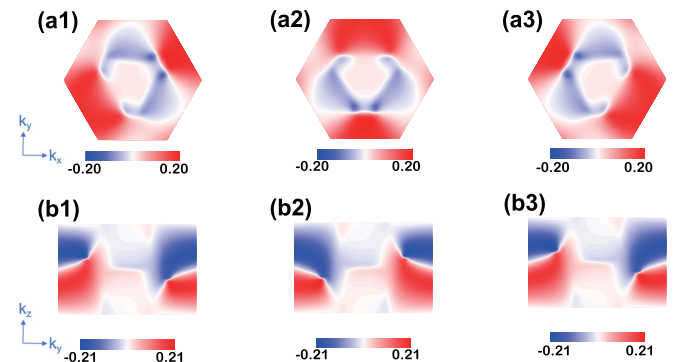


FIG. 4. Chiral phonons in Te. (a) Distributions of the phonon polarizations of the highest band on the plane $k_z a/2\pi = -\frac{1}{5}$ for sublattice Te1 s_1^z (a1), sublattice Te2 s_2^z (a2), and sublattice Te3 s_3^z (a3), respectively. (b) Distributions of the phonon polarizations of the highest band on the plane $k_y = \frac{\sqrt{3}}{3} k_x$ for sublattice Te1 s_1^z (b1), on the plane $k_x = 0$ for sublattice Te2 s_2^z (b2), and on the plane $k_y = -\frac{\sqrt{3}}{3} k_x$ for sublattice Te3 s_3^z (b3), respectively.

unit cell are threefold rotationally symmetrical along the z axis with one another. This implies a similar relationship among vibration modes in the z^\perp plane for the three atoms per unit cell. Therefore, in the following discussion, we mainly focus on the phonon effective magnetic field along the z direction. However, due to the difference in Born effective charge tensor of each sublattice, the phonon effective magnetic fields at a certain place i induced by each sublattice, i.e., β_{ij}^z , are also different. Here, we label sublattices Te1, Te2, and Te3 as $j = 1, 2, 3$. For the average phonon effective magnetic field at each sublattice per mode, that is $d_{ij}^\alpha = 0$ and $d_{ij}^\beta = 0$, we use $i = 1, 2, 3$ to represent the field at sublattice Te1, Te2, and Te3, respectively.

We then study the spatial distribution of the effective magnetic field β_{ij}^z . Taking the chiral motion of sublattice Te1 as an example, we focus on a phonon mode at $(ka/2\pi) = [\frac{1}{3}, \frac{1}{3}, -\frac{1}{5}]$ of the highest frequency band and plot the spatial distribution of the phonon effective magnetic field β_{i1}^z , as shown in Fig. 5(a). Because the effective charge $Z_{1,z^\perp}^* (\sigma = 9) = -0.44e$ is negative, the direction of a steady current is opposite to that of the phonon rotation motion. As can be seen in the inset, it shows that the direction of effective magnetic field can be determined by the right-hand grip rule. That is, curl your fingers along the direction of phonon current, then your thumb will point the direction of magnetic field inside the current trajectory. Outside the trajectory, the magnetic field has the opposite direction. For the specific phonon mode shown in Fig. 3(a), sublattice Te1 does right-handed polarized rotation in z^\perp plane with $r_{mi,1}^{z^\perp} = 0.040 \text{ \AA}$ and $r_{ma,1}^{z^\perp} = 0.133 \text{ \AA}$. As shown in Fig. 5(a), for planes with different heights $d_{i1}^{z^\perp} > 0$ from the z^\perp plane, the effective magnetic field increases and then decreases at two sides when the difference between $\tilde{r}_1^{z^\perp} \approx 0.073 \text{ \AA}$ and $d_{i1}^{z^\perp}$ is much larger, and continuously changes in the whole range. However, for the plane with $d_{i1}^{z^\perp} = 0$, as indicated by the bold line, the effective magnetic field monotonically decreases at two sides when $d^{z^\perp} < \tilde{r}_1^{z^\perp}$ or $d^{z^\perp} > \tilde{r}_1^{z^\perp}$, which results in the appearance of a singularity at $d^{z^\perp} = \tilde{r}_1^{z^\perp}$.

What is more, as can be seen along the arrow direction in Fig. 5(a), the effective magnetic field gradually weakens when $d_{i1}^{z^\perp}$ increases. If $d_{i1}^{z^\perp} \geq 2.0\tilde{r}_1^{z^\perp} \approx 0.146 \text{ \AA}$, β_{i1}^z will trend to zero. Moreover, along the $d_{i1}^{z^\perp}$ direction, β_{i1}^z is nearly zero when $d_{i1}^{z^\perp} \geq 2.0\tilde{r}_1^{z^\perp}$. From our calculations, as shown in Fig. 3, the maximum vibration amplitude of phonon in each band is usually on the order of 0.1 \AA for Te, twice of which is much smaller than the actual distance between different atoms which is on the order of 1 \AA . The vibration amplitude estimated here is consistent with previous calculations [50,56]. The temperature gradient here only causes an offset term in the Bose-Einstein distribution, and the small heat current does not change the amplitude (or radius) of each mode. This means that if we calculate the effective magnetic field at sublattice j , the effective magnetic field generated by the chiral motion of other Te atoms has almost no contribution at sublattice j . Therefore, we can assume that the magnetic field strength at each sublattice Te is only contributed by the field source at that sublattice.

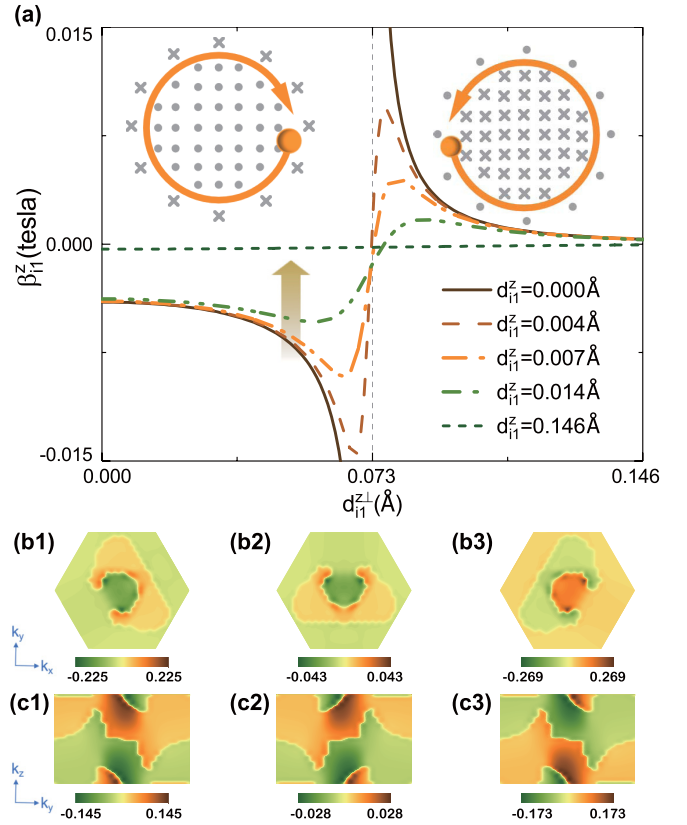


FIG. 5. Chiral phonon effective magnetic field of Te at k point. (a) Phonon effective magnetic field β_{i1}^z induced by Te1 as a function of the distance $d_{i1}^{z^\perp}$ for different $d_{i1}^{z^\perp}$ at $(ka/2\pi) = [\frac{1}{3}, \frac{1}{3}, -\frac{1}{5}]$ of the highest band. Here, $\tilde{r}_1^{z^\perp} = 0.073 \text{ \AA}$. The arrow indicates the increase of $d_{i1}^{z^\perp}$. Insets: schematic of the effective magnetic field produced by a left-handed (left panel) and a right-handed (right panel) phonon circular motions for a site with negative effective charge, respectively. Here, the effective magnetic field is perpendicular to the paper; the symbols used for the field pointing inward (like the tail of an arrow) and the field pointing outward (like the tip of an arrow). (b) Distributions of the chiral phonon effective magnetic field β_i^z of the highest band on the plane $k_z a/2\pi = -\frac{1}{5}$ at sublattice Te1 (b1), sublattice Te2 (b2), and sublattice Te3 (b3), respectively. The unit of bar is in tesla. (c) Distributions of the chiral phonon effective magnetic field β_i^z of the highest band on the plane $k_y = \frac{\sqrt{3}}{3}k_x$ for sublattice Te1 (c1), on the plane $k_x = 0$ at sublattice Te2 (c2), and on the plane $k_y = -\frac{\sqrt{3}}{3}k_x$ at sublattice Te3 (c3), respectively. The unit of bar is tesla. Here, $Z_{1,z^\perp}^* (\sigma = 9) = -0.44e$, $Z_{2,z^\perp}^* (\sigma = 9) = -0.09e$, and $Z_{3,z^\perp}^* (\sigma = 9) = 0.53e$.

Then, the distributions of chiral phonon-induced effective magnetic fields β_i^z at each sublattice in the Brillouin zone are calculated. Here, we take the plane $k_z a/2\pi = -\frac{1}{5}$ for the highest band as an example. As depicted in Figs. 5(b) and 5(c), the distribution of β_i^z shares the same symmetry with that of phonon polarizations shown in Fig. 4. If the phonon circular polarization is zero, the phonon mode will do linear vibration or remain still; otherwise, they do circular or elliptical rotation, and nonzero effective magnetic field β_i^z will be induced. Because the sublattice Te3 has an effective charge $Z_{3,z^\perp}^* (\sigma = 9)$ with the opposite sign of that of the other two sublattices,

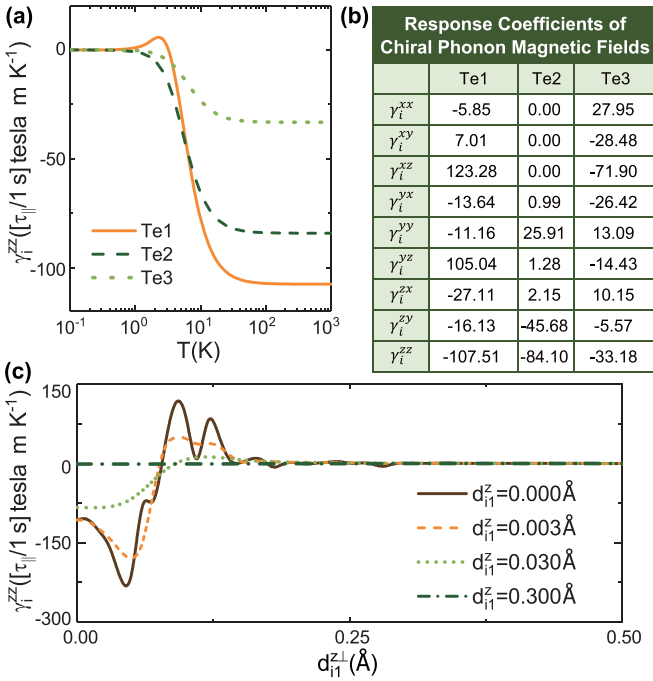


FIG. 6. Average chiral phonon effective magnetic field per mode of Te induced by a temperature gradient. (a) Response coefficient γ_i^{zz} of average chiral phonon effective magnetic field at each sublattice per mode induced by a temperature gradient as a function of temperature T . (b) Response coefficient $\gamma_i^{\alpha\alpha'}$ of average chiral phonon effective magnetic field at each sublattice per mode induced by a temperature gradient at room temperature. The unit of $\gamma_i^{\alpha\alpha'}$ is $(\tau/1\text{ s})\text{ T m K}^{-1}$. (c) Response coefficient γ_i^{zz} of average chiral phonon effective magnetic field at a place i near sublattice Te1 per mode induced by a temperature gradient as a function of the distance d_{i1}^z for different d_{i1}^z .

in addition to the rotational symmetry, the distribution of the effective magnetic field β_3^z also has an opposite sign. For a given chiral phonon trajectory, the effective magnetic field strength at each \mathbf{k} point induced by sublattice j is proportional to the corresponding effective charge $Z_{j,z\pm}^*$ (σ). Thus, the maximum β_3^z at sublattice Te3 shown in Figs. 5(b) and 5(c) is the largest among the three sublattices. Furthermore, because of the time-reversal symmetry, the chiral phonon-induced effective magnetic field β_i^z is an odd function in \mathbf{k} space, which is in accordance to the discussion in Sec. II. Therefore, in equilibrium, the average magnetic field induced by chiral phonon, i.e., $B_{i=j,eq}^\alpha$, is zero.

As indicated by Eq. (10), an average magnetic field of chiral phonon can be induced by a temperature gradient. Figure 6(a) shows the response coefficient γ_i^{zz} for the effective magnetic field at each sublattice j as a function of temperature T . At low temperature, γ_i^{zz} is almost 0. As the temperature increases, γ_i^{zz} will increase to a maximum value and eventually tends to a constant. The linear response coefficient is related to not only the offset term of the Bose-Einstein distribution shown in Eq. (9), but also the effective charge of the sublattice in each band. Therefore, there may be fluctuations with temperature before the response coefficient grows rapidly. Figure 6(b) lists the response coefficient at room

temperature. In the component of zz , γ_i^{zz} has the maximum value of $\gamma_1^{zz} = -107.51$ ($\tau_{\perp}/1\text{ s}$) T m K^{-1} . For sublattice Te2, due to the zero $Z_{2,xy}^*$ and $Z_{2,xz}^*$ [as listed in Fig. 2(c)], β_2^x is zero, thus giving rise to the zero $\gamma_2^{x\alpha}$, $\alpha = x, y, z$. The maximum linear response coefficient of average chiral phonon effective magnetic field at each sublattice at room temperature is $\gamma_1^{xz} = 123.28$ ($\tau_{\perp}/1\text{ s}$) T m K^{-1} .

When the place i deviates from the sublattice, as shown in Fig. 6(c), for small d_{i1}^z , the linear response coefficient first increases, then decreases to zero. For relatively larger d_{i1}^z on the order of 0.01 \AA , the linear response coefficient directly increases to the first zero point. After then, the coefficient increases again and then decreases; it finally tends to zero. It is worth noting that because β_{i1}^z is an odd function in \mathbf{k} space, under the condition of $d_{i1}^z = 0$, the divergence shown in Fig. 5(a) disappears in Fig. 6(c). If d_{i1}^z is on the order of 0.1 \AA , the effective magnetic field attenuates to zero. Since the distance between atoms is on the order of 1 \AA , the superposition of magnetic fields originated from other points will hardly enhance the effective magnetic field strength. From Refs. [34,57], the phonon relaxation time along and perpendicular to the c axis of Te can be set as $\tau_{\parallel} \sim 10\text{ ps}$ and $\tau_{\perp} \sim 1\text{ ps}$, respectively. We then set the temperature difference over the sample size D to be denoted by ΔT . Thus, the maximum average effective magnetic field of chiral phonons at a place i induced by temperature gradient can be estimated by

$$B_{i,neq}^{\alpha\alpha'} \sim -\frac{\Delta T/(1\text{ K})}{D/(1\text{ m})} \times 10^{-9}\text{ T} \quad (11)$$

at room temperature. Finally, $B_{i,neq}^{\alpha\alpha'}$ is estimated on the order of 10^{-2} T when $\Delta T = 10\text{ K}$ and $D = 1\text{ }\mu\text{m}$ at room temperature. In a real material, without external magnetic field, the effective magnetic field \mathbf{B} is related to the magnetization density by the vacuum permeability μ_0 , i.e., $\mathbf{B} = \mu_0\mathbf{M}$ [1]. Thus, at room temperature, the maximum phonon magnetization density can be estimated by

$$M_{neq}^{\alpha\alpha'} \sim -\frac{\Delta T/(1\text{ K})}{D/(1\text{ m})} \times 10^{-3}\text{ A m}^{-1}. \quad (12)$$

Therefore, at room temperature, if $\Delta T = 10\text{ K}$ and $D = 1\text{ }\mu\text{m}$, the maximum phonon magnetization density is estimated on the order of 10^4 A m^{-1} . This is much larger than previous calculations on the average phonon magnetization density per unit cell [34] because the phonon magnetic moment or the phonon magnetic field is greatly affected by the spatial distribution.

B. Spontaneous magnetization manipulated by chiral phonons

The chiral phonon-induced effective magnetic field we discovered may have potential in manipulation of spontaneous magnetization.

1. Spontaneous magnetization in a ferromagnetic material

In the Heisenberg model, for a ferromagnetic material [58], the coupling constant satisfies $J > 0$. We assume that the magnetic ions with N_{sp} spins S_{sp} are arranged in the lattice. According to the mean-field theory, the Heisenberg exchange interaction between one site and the other can be

approximately written as

$$\mathcal{H}^{sp} = -2ZJ\hat{S}_{sp} \cdot \langle \hat{S}_{sp} \rangle, \quad (13)$$

where $\hat{S}_{sp} = (\hat{S}_{sp}^x, \hat{S}_{sp}^y, \hat{S}_{sp}^z)$ is the spin operator, and Z is the coordination number. In the absence of an external magnetic field, an ordered spin state appears below the Curie temperature $T_C = \frac{2ZJ}{3k_B} S_{sp}(S_{sp} + 1)$. This is what we call spontaneous magnetization [51].

When an effective magnetic field \mathbf{B}_{neq} induced by chiral phonons is considered in the system, ferromagnets have a Zeeman energy of

$$\mathcal{H}^{ph} = -g\mu_B \mathbf{B}_{neq} \cdot \hat{S}_{sp}, \quad (14)$$

where g is the Landé factor and μ_B denotes the Bohr magneton. Assuming that the effective magnetic field is along the z direction, the Hamiltonian of each site can be given by

$$\mathcal{H}^z = -2ZJ\hat{S}_{sp}^z \langle \hat{S}_{sp}^z \rangle - g\mu_B B_{neq}^z \hat{S}_{sp}^z, \quad (15)$$

and the corresponding eigenvalue is

$$E_h = -h(2ZJ\langle \hat{S}_{sp}^z \rangle + g\mu_B B_{neq}^z), \quad h = 0, \pm 1, \dots, \pm S_{sp}. \quad (16)$$

Thus, the spontaneous magnetization can be obtained by

$$M(T) = N_{sp}g\mu_B \langle \hat{S}_{sp}^z \rangle = M(0)B_S(x), \quad (17)$$

where $\langle \hat{S}_{sp}^z \rangle = \frac{\sum_{h=-S_{sp}}^{S_{sp}} h e^{-E_h/(k_B T)}}{\sum_{h=-S_{sp}}^{S_{sp}} e^{-E_h/(k_B T)}}$, $M(0) = N_{sp}g\mu_B S_{sp}$ is the saturation magnetization at zero temperature, and $B_S(x) = \frac{2S_{sp}+1}{2S_{sp}} \coth(\frac{2S_{sp}+1}{2S_{sp}}x) - \frac{1}{2S_{sp}} \coth(\frac{1}{2S_{sp}}x)$, $x = -\frac{E_h S_{sp}}{hk_B T}$ is the Brillouin function. Thus, the critical temperature becomes

$$T'_C = T_C - \frac{g\mu_B S_{sp}}{k_B x} B_{neq}^z. \quad (18)$$

Therefore, the effective magnetic fields generated by circular rotations of chiral phonons have the ability to tune the Curie temperature, leading to the manipulation of spontaneous magnetization in ferromagnetic materials.

2. Phonon torque and spontaneous magnetization in a general material

In a general material, even if it is not a magnetic material, the phonon effective magnetic field is also expected to be applied, but further research is still needed. Here, we just propose an assumption.

In classical mechanics, the net torque on a rigid-body determines the derivative of corresponding angular momentum with respect to time [59]. In a microscopic picture, because the angular momentum of phonons has been reported [44], the phonon torque between sublattice j and sublattice j' in unit cell n can be defined as

$$\mathbf{Q}_{j,j'} = \sum_n \mathbf{u}_{nj} \times \mathbf{F}_{nj,nj'}, \quad (19)$$

where \mathbf{u}_{nj} is the displacement and $\mathbf{F}_{nj,nj'}$ is the force from sublattice j' acting on the other sublattice j . Thus, along the z direction, the magnitude of phonon torque is $Q_{j,j'}^z = \sum_n (u_{nj}^x F_{nj,nj'}^y - u_{nj}^y F_{nj,nj'}^x)$. Here, $F_{nj,nj'}^\alpha = -\sum_\beta K_{nj,nj'}^{\alpha\beta} u_{nj}^\beta$,

which is the α th component of $\mathbf{F}_{nj,nj'}$. If we set $u_{nj} = (u_{nj}^x, u_{nj}^y)^T$, then

$$Q_{j,j'}^z = \sum_n u_{nj}^T \kappa_{nj,nj'} u_{nj}, \quad (20)$$

where $\kappa_{nj,nj'} = \begin{bmatrix} -K_{nj,nj'}^{yx} & -K_{nj,nj'}^{yy} \\ K_{nj,nj'}^{xx} & K_{nj,nj'}^{xy} \end{bmatrix}$. To obtain the torque of chiral phonon, we can set $\epsilon_j(k) = (A_j^x \cos \theta_j^x, A_j^y \cos \theta_j^y)^T$. By using the second quantization for u_{nj} as $u_{nj} = \sum_k \epsilon_j(k) e^{i(\mathbf{R}_n \cdot \mathbf{k} - \omega_k t)} \sqrt{\frac{\hbar}{2\omega_k N_{\text{cell}} m_j}} a_k + \text{H.c.}$ with $k = (\mathbf{k}, \sigma)$ denoting a wave vector \mathbf{k} and a branch σ , \mathbf{R}_n representing the center equilibrium position of the n th unit cell, and N_{cell} is the number of the unit cells, the phonon torque can be written as

$$\begin{aligned} Q_{j,j'}^z &= \frac{\hbar}{2\sqrt{m_j m_{j'}}} \sum_{k,k'} \frac{1}{\sqrt{\omega_k \omega_{k'}}} [\epsilon_j^\dagger(k) \kappa_{nj,nj'} \epsilon_{j'}(k') \\ &\quad + \epsilon_j(k')^T \kappa_{nj,nj'} \epsilon_j^*(k)] \delta_{k',k} a_k^\dagger a_k e^{i(\omega_k - \omega_{k'})t} \\ &\quad + \frac{\hbar}{2\sqrt{m_j m_{j'}}} \sum_k \frac{\epsilon_j(k)^T \kappa_{nj,nj'} \epsilon_j^*(k)}{\omega_k}. \end{aligned} \quad (21)$$

In equilibrium, the torque of chiral phonon can be simplified as

$$\begin{aligned} Q_{j,j'}^z &= \sum_k \mu_{j,j'}^z(k) \left[f(\omega_k) + \frac{1}{2} \right], \\ \mu_{j,j'}^z(k) &= \frac{\hbar \epsilon_j^\dagger(k) \kappa_{nj,nj'} \epsilon_j(k)}{\omega_k \sqrt{m_j m_{j'}}}. \end{aligned} \quad (22)$$

Here, $\mu_{j,j'}^z(k)$ is the phonon torque of branch σ at wave vector \mathbf{k} .

Assuming that both sublattices do circularly polarized motion, a nonzero $\mu_{j,j'}^z(k)$ occurs. This means that there may be certain interactions between chiral phonons. We assume that the interaction is similar to Eq. (13), that is,

$$\mathcal{H}^{ch} \sim P \hat{S}_{ph} \cdot \langle \hat{S}_{ph} \rangle, \quad (23)$$

where P is the coupling constant between chiral phonons and \hat{S}_{ph} is the chiral phonon operator. When an effective magnetic field of chiral phonon is taken into consideration, an additional energy takes place. Finally, in analogy to Sec. IV B 1, the effective magnetic fields induced by chiral phonon may also have the ability to induce the spontaneous magnetization in a general material.

V. CONCLUSION

In summary, under the Born-Oppenheimer approximation, we have theoretically predicted and estimated the effective magnetic fields induced by chiral phonons in the point-charge model using the Biot-Savart law. For tellurium, when applying a temperature gradient, an average effective magnetic field per mode for a specific location within a unit cell can appear on the order of 0.01 T at room temperature. Since the effective magnetic field disappears at a distance on the order of 0.1 Å from the field source, it is impossible to increase its strength by stacking atomic layers. The chiral phonon

effective magnetic fields found in this work have the capacity of manipulating the Curie temperature in a ferromagnetic material, and thus have great importance in the spontaneous magnetization manipulation. If there is certain interaction between chiral phonons, the effective magnetic field may also induce the spontaneous magnetization in a general material.

As a final remark, it is needed to be noticed that, here, we only consider a preliminary point-charge model. The influence of charge distribution on the effective magnetic field by considering the mode-dependent relaxation time and the accurate calculation of the magnetic field still needs to be further studied.

Note added. Recently, we noticed that a similar phenomenon on effective phonon magnetic fields induced magnetization has been reported in cerium trichloride via a laser pulse [60].

ACKNOWLEDGMENTS

We acknowledge support from NSFC (Grants No. 11890703 and No. 12005105) and the China Scholarship Council (award to G. Xiong for one year's study abroad at the National University of Singapore). We thank J. Zhou, X. Li, and Z. Yu for the helpful discussions.

-
- [1] D. J. Griffiths, *Introduction to Electrodynamics*, 4th ed. (Pearson, New York, 2005).
- [2] L. D. Landau and E. M. Lifshitz, *Electrodynamics of Continuous Media* (Pergamon, New York, 1960), Vol. 8.
- [3] C. B. Williams and R. B. Yates, *Sens. Actuators, A* **52**, 8 (1996).
- [4] J. H. Harlow, *Electric Power Transformer Engineering* (CRC Press, Boca Raton, FL, 2003).
- [5] J. C. Mallinson, *The Foundations of Magnetic Recording* (Academic, New York, 2012).
- [6] J. Ongena, R. Koch, R. Wolf, and H. Zohm, *Nat. Phys.* **12**, 398 (2016).
- [7] J. D. Jackson, *Classical Electrodynamics* (Wiley, New York, 1999).
- [8] J. Li, J. Liu, S. A. Baronett, M. Liu, L. Wang, R. Li, Y. Chen, D. Li, Q. Zhu, and X.-Q. Chen, *Nat. Commun.* **12**, 1204 (2021).
- [9] Y. Liu, X. Chen, and Y. Xu, *Adv. Funct. Mater.* **30**, 1904784 (2020).
- [10] L. Du, J. Tang, Y. Zhao, X. Li, R. Yang, X. Hu, X. Bai, X. Wang, K. Watanabe, T. Taniguchi *et al.*, *Adv. Funct. Mater.* **29**, 1904734 (2019).
- [11] N. Li, J. Ren, L. Wang, G. Zhang, P. Hänggi, and B. Li, *Rev. Mod. Phys.* **84**, 1045 (2012).
- [12] H. Zhu, J. Yi, M.-Y. Li, J. Xiao, L. Zhang, C.-W. Yang, R. A. Kaindl, L.-J. Li, Y. Wang, and X. Zhang, *Science* **359**, 579 (2018).
- [13] L. Zhang and Q. Niu, *Phys. Rev. Lett.* **115**, 115502 (2015).
- [14] H. Chen, W. Wu, J. Zhu, S. A. Yang, and L. Zhang, *Nano Lett.* **21**, 3060 (2021).
- [15] T. Yin, K. A. Ulman, S. Liu, A. Granados del Águila, Y. Huang, L. Zhang, M. Serra, D. Sedmidubsky, Z. Sofer, S. Y. Quek *et al.*, *Adv. Mater.* **33**, 2101618 (2021).
- [16] J. Kishine, A. S. Ovchinnikov, and A. A. Tereshchenko, *Phys. Rev. Lett.* **125**, 245302 (2020).
- [17] W. Zhang, A. Srivastava, X. Li, and L. Zhang, *Phys. Rev. B* **102**, 174301 (2020).
- [18] H. Chen, W. Wu, S. A. Yang, X. Li, and L. Zhang, *Phys. Rev. B* **100**, 094303 (2019).
- [19] C. Chen, X. Chen, B. Deng, K. Watanabe, T. Taniguchi, S. Huang, and F. Xia, *Phys. Rev. B* **103**, 035405 (2021).
- [20] Y. Tatsumi, T. Kaneko, and R. Saito, *Phys. Rev. B* **97**, 195444 (2018).
- [21] C. M. Gilardoni, F. Hendriks, C. H. van der Wal, and M. H. D. Guimarães, *Phys. Rev. B* **103**, 115410 (2021).
- [22] A. Delhomme, D. Vaclavkova, A. Slobodeniuk, M. Orlita, M. Potemski, D. Basko, K. Watanabe, T. Taniguchi, D. Mauro, C. Barreateau *et al.*, *2D Mater.* **7**, 041002 (2020).
- [23] M. He, P. Rivera, D. Van Tuan, N. P. Wilson, M. Yang, T. Taniguchi, K. Watanabe, J. Yan, D. G. Mandrus, H. Yu *et al.*, *Nat. Commun.* **11**, 618 (2020).
- [24] Z. Li, T. Wang, S. Miao, Z. Lian, and S.-F. Shi, *Nanophotonics* **9**, 1811 (2020).
- [25] Z. Li, T. Wang, S. Miao, Y. Li, Z. Lu, C. Jin, Z. Lian, Y. Meng, M. Blei, T. Taniguchi *et al.*, *Nat. Commun.* **11**, 1 (2020).
- [26] Q. Guo, T. Fu, J. Tang, D. Pan, S. Zhang, and H. Xu, *Phys. Rev. Lett.* **123**, 183903 (2019).
- [27] Z. Li, T. Wang, C. Jin, Z. Lu, Z. Lian, Y. Meng, M. Blei, M. Gao, T. Taniguchi, K. Watanabe *et al.*, *ACS Nano* **13**, 14107 (2019).
- [28] Z. Li, T. Wang, C. Jin, Z. Lu, Z. Lian, Y. Meng, M. Blei, S. Gao, T. Taniguchi, K. Watanabe *et al.*, *Nat. Commun.* **10**, 2469 (2019).
- [29] E. Liu, J. van Baren, T. Taniguchi, K. Watanabe, Y.-C. Chang, and C. H. Lui, *Phys. Rev. Res.* **1**, 032007(R) (2019).
- [30] X. Chen, X. Lu, S. Dubey, Q. Yao, S. Liu, X. Wang, Q. Xiong, L. Zhang, and A. Srivastava, *Nat. Phys.* **15**, 221 (2019).
- [31] T. Saito, K. Misaki, H. Ishizuka, and N. Nagaosa, *Phys. Rev. Lett.* **123**, 255901 (2019).
- [32] A. V. Inyushkin and A. Taldenkov, *JETP Lett.* **86**, 379 (2007).
- [33] C. Strohm, G. L. J. A. Rikken, and P. Wyder, *Phys. Rev. Lett.* **95**, 155901 (2005).
- [34] M. Hamada, E. Minamitani, M. Hirayama, and S. Murakami, *Phys. Rev. Lett.* **121**, 175301 (2018).
- [35] S. Park and B.-J. Yang, *Nano Lett.* **20**, 7694 (2020).
- [36] D. M. Juraschek and N. A. Spaldin, *Phys. Rev. Mater.* **3**, 064405 (2019).
- [37] R. M. Geilhufe, [arXiv:2108.03473](https://arxiv.org/abs/2108.03473).
- [38] R. M. Geilhufe, V. Juričić, S. Bonetti, J.-X. Zhu, and A. V. Balatsky, *Phys. Rev. Res.* **3**, L022011 (2021).
- [39] B. Cheng, T. Schumann, Y. Wang, X. Zhang, D. Barbalas, S. Stemmer, and N. Armitage, *Nano Lett.* **20**, 5991 (2020).
- [40] D. M. Juraschek, P. Narang, and N. A. Spaldin, *Phys. Rev. Res.* **2**, 043035 (2020).
- [41] D. M. Juraschek, M. Fechner, A. V. Balatsky, and N. A. Spaldin, *Phys. Rev. Mater.* **1**, 014401 (2017).
- [42] T. F. Nova, A. Cartella, A. Cantaluppi, M. Först, D. Bossini, R. V. Mikhaylovskiy, A. V. Kimel, R. Merlin, and A. Cavalleri, *Nat. Phys.* **13**, 132 (2017).

- [43] A. Baydin, F. G. G. Hernandez, M. Rodriguez-Vega, A. K. Okazaki, F. Tay, G. T. Noe, I. Katayama, J. Takeda, H. Nojiri, P. H. O. Rappl, E. Abramof, G. A. Fiete, and J. Kono, *Phys. Rev. Lett.* **128**, 075901 (2022).
- [44] L. Zhang and Q. Niu, *Phys. Rev. Lett.* **112**, 085503 (2014).
- [45] M. Hamada and S. Murakami, *Phys. Rev. B* **101**, 144306 (2020).
- [46] K. Dunnett, J.-X. Zhu, N. A. Spaldin, V. Juričić, and A. V. Balatsky, *Phys. Rev. Lett.* **122**, 057208 (2019).
- [47] Y. Ren, C. Xiao, D. Saporov, and Q. Niu, *Phys. Rev. Lett.* **127**, 186403 (2021).
- [48] A. Zabalo, C. E. Dreyer, and M. Stengel, *Phys. Rev. B* **105**, 094305 (2022).
- [49] X. Gonze and C. Lee, *Phys. Rev. B* **55**, 10355 (1997).
- [50] M. T. Dove and M. T. Dove, *Introduction to Lattice Dynamics* (Cambridge University Press, Cambridge, 1993), Vol. 4.
- [51] N. W. Ashcroft, and N. D. Mermin, *Solid State Physics* (Harcourt College, New York, 1976).
- [52] G. Kresse and J. Furthmüller, *Comput. Mater. Sci.* **6**, 15 (1996).
- [53] P. E. Blöchl, *Phys. Rev. B* **50**, 17953 (1994).
- [54] J. P. Perdew, K. Burke, and M. Ernzerhof, *Phys. Rev. Lett.* **77**, 3865 (1996).
- [55] R. M. Pick, M. H. Cohen, and R. M. Martin, *Phys. Rev. B* **1**, 910 (1970).
- [56] P. Boolchand, B. Robinson, and S. Jha, *Phys. Rev. B* **2**, 3463 (1970).
- [57] X. Wu, J. Lee, V. Varshney, J. L. Wohlwend, A. K. Roy, and T. Luo, *Sci. Rep.* **6**, 1 (2016).
- [58] C. Kittel and C.-Y. Fong, *Quantum Theory of Solids* (Wiley, New York, 1963), Vol. 5.
- [59] L. D. Landau and E. M. Lifshitz, *Mechanics*, 3rd ed. (Elsevier, Oxford, 1976), Vol. 1.
- [60] D. M. Juraschek, T. Neuman, and P. Narang, *Phys. Rev. Res.* **4**, 013129 (2022).